Research Article | Vol. 29, No. 10 / 10 May 2021 / Optics Express 14649
Optics EXPRESS

Loss-coupled DFB nano-ridge laser monolithically grown on a standard 300-mm Si wafer

YUTING SHI,[1] MARIANNA PANTOUVAKI,[2] JORIS VAN CAMPENHOUT,[2] DAVIDE COLUCCI,[1,2] MARINA BARYSHNIKOVA,[2] BERNARDETTE KUNERT,[2] AND DRIES VAN THOURHOUT[1,2,*]

[1]*INTEC, Ghent University, Technologiepark-Zwijnaarde 126, 9052 Ghent, Belgium*
[2]*IMEC, Kapeldreef 75, 3001 Heverlee, Belgium*
[*]*Dries.VanThourhout@UGent.be*

Abstract: We present a loss-coupled distributed feedback microlaser, monolithically grown on a standard 300-mm Si wafer using nano-ridge engineering. The cavity is formed by integrating a metallic grating on top of the nano-ridge. This allows forming a laser cavity without etching the III-V material, avoiding damaged interfaces and the associated carrier loss. Simulations, supported by experimental characterisation of the modal gain of the nano-ridge devices, predict an optimal duty cycle for the grating of ~0.4, providing a good trade-off between coupling strength and cavity loss for the lasing mode. The model was experimentally verified by characterising the lasing threshold and external efficiency of devices exhibiting gratings with varying duty cycle. The high modal gain and low threshold obtained prove the excellent quality of the epitaxial material. Furthermore, the low loss metal grating might provide a future route to electrical injection and efficient heat dissipation of these nanoscale devices.

1. Introduction

Silicon photonics is considered to be one of the key technology platforms in meeting the future requirements of power-efficient and high-density interconnects but the lack of an efficient and cost-efficient light source directly integrated with the platform remains a bottleneck. Si, as an indirect-bandgap semiconductor, is a poor light emitter. Direct-bandgap semiconductors such as GaAs and InP on the other hand, have proven to be highly efficient in light generation but their integration on Si remains a huge challenge, given the large lattice mismatch between silicon (a_{Si} = 5.431 Å) and most direct bandgap III–V compounds(from 5.6 Å to 6.5 Å). Often there is also a large difference in thermal expansion coefficients. To bypass these issues, integration approaches based on wafer bonding [1–4] and transfer printing [5–7] have been developed. Nevertheless, the direct epitaxial growth of III-V materials, is widely believed to be the ultimate solution towards cost-effective laser integration on the silicon photonics platform. Therefore, several groups have developed novel epitaxial processes providing high quality III-V materials directly grown on silicon substrates [8–11]. In one group of approaches, confined growth in a trench or V-groove is used to suppress defects. This allows to reduce the thickness of the required buffer layer considerably, providing prospects for coupling light with waveguides defined on the same substrate. Several groups of demonstrated lasing under optical pumping in such devices [12,13]. Thus far, the nano-scale dimensions of these devices are a potential hinder to electrical pumping in terms of efficient light emission, as the closely positioned metal contacts would result in unacceptable modal loss. Therefore, in this paper, we report a partly loss-coupled (PLC) distributed feedback (DFB) nano-ridge laser, which does provide a route towards electrical injection of these nanoscale lasers.

#422245 https://doi.org/10.1364/OE.422245
Journal © 2021 Received 12 Feb 2021; revised 14 Apr 2021; accepted 22 Apr 2021; published 28 Apr 2021

Optics EXPRESS

The reported PLC DFB nano-ridge laser is monolithically grown on a standard 300-mm Si wafer through aspect ratio trapping and nanoridge engineering [14]. The detailed heteroepitaxy process [15] and material characterisation [16] were described elsewhere, and in [17] we proposed an approach to interface these nano-ridge devices with silicon waveguides. In initial work, we also showed lasing from devices with an etched grating forming a $\lambda/4$ phase-shift DFB cavity [13] defined on top.

In this paper, starting from this work, we measure for the first time the modal gain of the nano-ridge material, using the variable stripe length (VSL) method, thereby providing a systematic understanding of the material relevant for future device design and application. Starting from this study we then designed PLC DFB lasers with a metal grating forming the DFB cavity. By carefully selecting the duty cycle of the metal grating, the modal loss of the lasing mode is reduced to 23 dB/cm (compared to >300dB/cm for a continuous metal contact). This design provides a good trade-off between the coupling strength provided by the grating and the cavity loss of the lasing mode. The PLC DFB nano-ridge shows single-mode lasing under optical pumping, with the measured threshold vs. duty cycle curve showing a good fit with our analytical model. Compared to an etched grating, the metallic grating cavity allows to avoid material damage and related carrier loss induced by the etching process, but also has the potential to serve as a pathway for electrical pumping the device in the future.

2. Laser design

Figure 1(a) shows a SEM image of the nano-ridge array. The height and width of the nano-ridge are measured to be 600 nm and 460 nm respectively. These dimensions are controlled through optimizing the growth conditions, and chosen such that the nanoridge can support a low-loss mode strongly confined in the InGaAs QWs. This is also obvious from Fig. 1(b), which shows the optical field distribution of the TE-like ground mode $E_{TE}(x, y)$ of the nano-ridge calculated by a finite difference eigenmode (FDE) solver. This TE mode exhibits the highest confinement in the QWs among all optical modes with $\Gamma_{QW} = 9.3\%$ and a negligible Si leakage loss of α_{leak}<5 dB/cm. More details on the nano-ridge geometry can be found in [13].

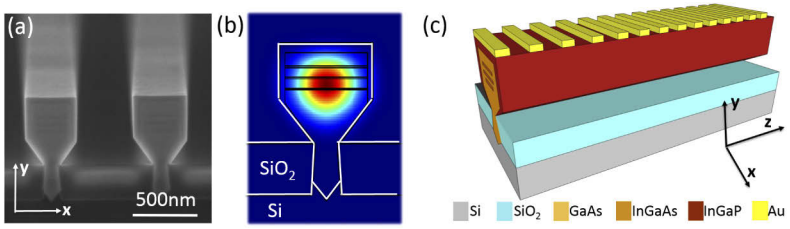

Fig. 1. (a) SEM image of the nano-ridge cross-section. (b) The lowest order TE-like optical mode $E_{TE}(x, y)$ calculated by a finite difference eigenmode (FDE) solver. The three QW regions are outlined by black lines. (c) Schematic diagram of the nano-ridge DFB device with metallic grating on top.

To allow for electrical injection, a metallic top contact is required. A standard top contact, covering the full nanoridge, would lead to unacceptably high losses, inhibiting laser operation. E.g. for a continuous gold top contact (thickness $h_{Au} = 40$ nm) the calculated modal loss for the lowest order TE mode is as high as $\alpha_{TE}(x, y) = 74cm^{-1}$(320 dB/cm).

Therefore we propose the alternative configuration illustrated in Fig. 1(c). A periodic metallic grating with period Λ on the top of the nano-ridge reduces the metal-induced loss while at the same time providing sufficient feedback to form a DFB cavity. Given the complex refractive index of Au ($n_{Au} = 0.242 - i6.704$) introduces changes both in the real and imaginary part of the effective refractive index of the TE-like ground mode $E_{TE}(x, y)$, the resulting cavity is

Optics EXPRESS

partly index-coupled and partly loss-coupled, hence we call the device a "PLC-DFB-laser". For a standard, fully index-coupled DFB cavity, there are two resonant modes, related to the two first-order Bloch modes. The two Bloch modes form a standing-wave pattern in the cavity, with identical period but a half-period shift from each other [18], as shown in Fig. 2(a). In a pure index-coupled DFB cavity, high side-mode-suppression-ratio (SMSR) lasing can be achieved by creating an extra phase shift inside the cavity or applying reflection coatings at the facet. A partly loss-coupled (PLC) cavity on the other hand has an inherent mode selection mechanism. The electrical field of the Bloch mode centered in the metal part "feels" more loss compared to the one centered in the dielectric part, and will be strongly suppressed. Simulation results (Fig. 2(a), duty cycle 0.5) show that the low-loss Bloch mode $E_{BL}(x, y, z)$ overlaps considerably less with the Au-grating than the high-loss Bloch mode $E_{BH}(x, y, z)$. Calculations show that the confinement factor (CF) in the gold layer of $E_{BL}(x, y, z)$ is indeed about ten times lower than that for $E_{BH}(x, y, z)$, which implies also the mode loss is ten times smaller. Consequently, $E_{BL}(x, y, z)$ having substantially lower loss will win the mode competition ensuring single-mode laser operation without need for a $\lambda/4$ shift section or facet coating.

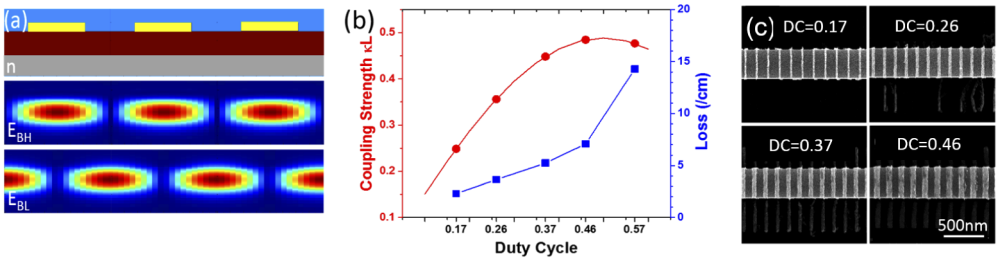

Fig. 2. (a) The refractive index profile and the field distribution of the two first-order Bloch modes along the PLC-DFB. On top the high-loss mode E_{BH}, below the low-loss mode E_{BL}. (b) Calculated coupling strength and loss of a metallic grating with length of 300 μm as a function of grating duty cycle. (c) Top-view SEM images of PLC-DFB lasers with measured grating duty cycle DC=0.17, 0.26, 0.37, 0.46 respectively.

The optical loss of mode $E_{BL}(x, y, z)$ can be reduced further by lowering the duty cycle $\frac{\Lambda_{Au}}{\Lambda}$ (Λ_{Au} the width of the Au sections within one period), yet doing so the grating strength is also weakened, reducing the coupling between the forward and backward lasing modes in the DFB cavity. Therefore the duty cycle of the metallic gratings has to be carefully designed, to reach a good trade-off between the cavity loss felt by the lasing mode and the coupling strength provided by the periodically patterned metallic layer [19]. Hence calculation of the cavity loss and coupling strength (κL) versus the grating duty cycle is needed.

First, we optimised the period of the grating to ensure overlap of its bandgap with the nanoridge gain spectrum centred around 1020 nm [13], using a commercial FDTD solver [20]. For a duty cycle of 0.5, we found $\Lambda = 164$ nm as the optimal grating period. Fixing the grating period and varying the duty cycle, we can now calculate the loss of the cavity mode $E_{BL}(x, y, z)$ as:

$$\alpha_{BL} = \Gamma_{Au}(x, y, z) \cdot \alpha_{Au}, \tag{1}$$

where $\Gamma_{Au}(x, y, z)$ is the 3D-confinement factor of the cavity mode in Au and α_{Au} the loss of Au at the resonant wavelength 1020 nm with $\alpha_{Au} = 8.18 \times 10^5$ cm^{-1}. The confinement factor Γ_{Au} is found from:

$$\Gamma_{Au}(x, y, z) = \frac{\int_0^{\Lambda_{Au}} \int_h^{h+\Delta h_{Au}} \int_{-w_{Au}/2}^{w_{Au}/2} |E_{BL}(x, y, z)|^2 dxdydz}{\iiint |E_{BL}(x, y, z)|^2 dxdydz}, \tag{2}$$

where W_{Au} is the width of the Au grating, i.e. the width of the nano-ridge. The calculated mode loss α_{BL} as a function of duty cycle $\frac{\Lambda_{Au}}{\Lambda}$ is plotted in Fig. 2(b). As expected, α_{BL} increases with

Optics EXPRESS

duty cycle and dramatically raises when $\frac{\Lambda_{Au}}{\Lambda}$>0.5, where the metal starts to occupy the majority of the nano-ridge surface.

For a DFB cavity, the total coupling strength κL is the product of the coupling coefficient κ and the length of the cavity L. In our case, L is fixed at 300 μm, restricted by the size of the pump spot. The coupling coefficient κ is a function of duty cycle $\frac{\Lambda_{Au}}{\Lambda}$ and the modulation depth $\Delta\varepsilon$, and can be approximated as

$$\kappa = \frac{k_0^2}{2\beta}\frac{sin(\pi\frac{\Lambda_{Au}}{\Lambda})}{\pi}\Delta\varepsilon\Gamma_{Au}(x,y) \tag{3}$$

assuming a rectangular grating pattern [19,21]. Note that $\Gamma_{Au}(x,y)$ is the 2D-confinement of the transversal mode $E_{TE}(x,y)$ in the 40 nm thick Au layer and is different from the 3D-confinement factor $\Gamma_{Au}(x,y,z)$ defined above. The other parameters in this equation are $k_0 = \frac{2\pi}{\lambda_0}$, the free-space wave vector, and $\beta = n_{eff}k_0$, the propagation constant of mode $E_{TE}(x,y)$, $\Delta\varepsilon = \varepsilon_{Au} - \varepsilon_{air} = (n_{Au} + ik_{Au})^2 - (n_{air} + ik_{air})^2 = 45.88 - i3.244$. Because the real part of ε is much larger than its imaginary part, we will ignore the imaginary part and let $\Delta\varepsilon \approx 45.88$ when calculating κ and the laser threshold I_{th} below. The calculated coupling strength κL as a function of duty cycle $\frac{\Lambda_{Au}}{\Lambda}$ is plotted in Fig. 2(b). κL is a sinusoidal function of the duty cycle, which first increases and then reaches a maximum when $\frac{\Lambda_{Au}}{\Lambda} = 0.5$ as expected. For $\frac{\Lambda_{Au}}{\Lambda}$>0.5 the modulation becomes less efficient again, resulting in a decrease of κL.

It is straightforward to speculate that the lowest laser threshold is held by a grating duty cycle no more than 0.5, as both the cavity loss and the coupling strength deteriorate for a duty cycle larger than 0.5. To calculate the optical threshold gain g_{th}, the calculated cavity loss α_{BL} and coupling coefficient κ and cavity length L can be plugged in the expression [22]:

$$\frac{|\kappa|^2}{(q+\Delta\beta)^2}e^{i2qL} = 1, \tag{4}$$

where

$$\Delta\beta = \kappa - i\frac{g_{th} - \alpha_{BL}}{2}, \tag{5}$$

$$q = \sqrt{\Delta\beta^2 - |\kappa|^2}. \tag{6}$$

These are applicable for a DFB laser without end facet reflection and with κ a real value. As already mentioned, the imaginary part of κ is ignored for simplicity. As for facet reflection, although the gratings continue beyond the pump region, it is considered negligible because outside the PLC cavity the absorption length is calculated to be ~ 7 μm while the cavity length is 300 μm.

3. Optical gain characterization

After having calculated the required modal gain at threshold g_{th} in Section 2., now the threshold pump intensity I_{th} can be estimated if the relation $g_m(I)$ describing the modal gain vs. pump intensity I is known. More importantly, the optical modal gain is recognized to be a significant parameter in evaluating the crystalline quality of the material. Nevertheless, there are only very few reports on the characterisation of the optical gain of III-V materials epitaxially grown on Silicon. Therefore, to get a more comprehensive understanding of the InGaAs/GaAs nano-ridge material, its optical gain is characterized using a variable stripe length (VSL) method [23,24]. This method allows extracting the optical gain of the GaAs nano-ridges over a wide range of pumping conditions.

The measurement setup, schematically shown in Fig. 3(a), consists of a Nd:YAG nanosecond pulsed laser (7 ns pulse width, 938 Hz repetition rate, 532 nm wavelength) pumping the nano-ridges from the top. A variable rectangular slit inserted in the beam path allows to control

Optics EXPRESS

the length of the pumped region from 10 to 200 μm. The pump intensity is controlled by a combination of a polarizer and a rotating half-wave plate (HWP). The signal is collected from a cleaved facet of the nano-ridge through a lensed fiber connected to an optical powermeter. The raw experimental data is the emission power as a function of the pump length at different pump intensities. For a given pump intensity, the measured signal is dominated by spontaneous emission (SE) for short pump lengths and then overtaken by amplified spontaneous emission (ASE) with increasing pump length. The signal saturates when further increasing the pump length. The pump-length-dependent emission can be described by the following equation [24]:

$$g_m \cdot L = \alpha(I_s - I_b) + \ln[\beta(I_s - I_b) + 1]. \tag{7}$$

with g_m the net modal gain, L the pump length, I_s the collected signal through the powermeter, I_b the background signal, α describing the gain saturation process and β a parameter related to the spontaneous emission. By fitting the experimental data using this equation, the modal gain g_m can be extracted. Through repeating this procedure for all pump intensities, the pump-intensity-dependent modal gain can be obtained, as plotted in Fig. 3(b). The compressively strained QWs are expected to strongly favor TE-polarised emission [25]. Taking into account that the TE-like ground mode $E_{TE}(x, y)$ has the smallest leakage loss and the highest confinement $\Gamma_{QW}(x, y)$ in the QWs, it is believed to be the dominant optical mode. The net modal gain $g_m = \Gamma_{QW}(x, y) \cdot g - \alpha_i$ not only incorporates the modal gain g but also the intrinsic nano-ridge loss α_i originating e.g. from leakage into the Si substrate and scattering. Therefore with $g_m \approx 460$ cm^{-1} at 300 kW/cm^2, the material gain g can be estimated to be above 5000 cm^{-1}, which is comparable with conventional GaAs material. To obtain an analytical expression for the net modal gain (g_m) vs. pump intensity (I), the experimental data is fitted with the expression [26] $g_m(I) = g_0 \cdot ln(I/I_0)$, with fit parameters $g_0 = 123.0$ cm^{-1}, $I_0 = 8.7$ kW/cm^2. This relation is plotted in Fig. 3(b) as the dashed red line.

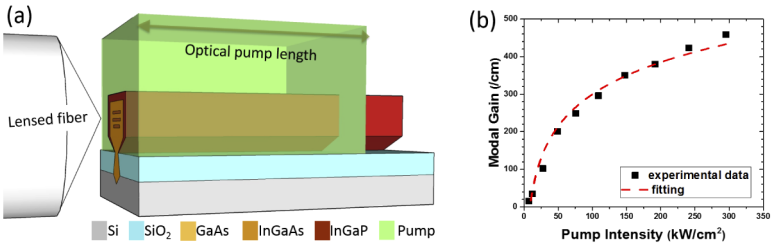

Fig. 3. (a) Schematic diagram of the setup used for characterisation of the optical gain. A variable length of the nano-ridge is pumped while the ASE is picked up from the edge facet. (b) Modal gain of the InGaAs/GaAs nano-ridges at different pump intensity levels. Black squared dots are the data extracted from the VSL experiment at different pump intensities while the red dashed line is the fit to the experimental data.

Having calculated the cavity optical loss α_{BL} and the coupling strength κL, and having the relation $g_m(I)$ experimentally obtained, the expected threshold pump intensity I_{th} as a function of the grating duty cycle can be derived by substituting these parameters into Eqs. (4) to 7. The result, depicted in Fig. 5(c) with triangular symbols, shows there is an optimal duty cycle at around 0.4 where the metal grating provides sufficiently strong coupling while only introducing a relative weak loss to the cavity mode, resulting in the lowest threshold intensity.

4. Device fabrication and characterization

To verify the theoretical calculations experimentally, we have fabricated a series of PLC-DFB devices with the duty cycle $\frac{\Lambda_{Au}}{\Lambda}$ of the metallic grating varying from 0.2 to 0.6 with an interval of

Optics EXPRESS

0.1 to cover the estimated optimal value. The physical length of the gratings is 600 μm, however, the effective cavity length is determined by the optical excitation window, which is $L = 300\ \mu$m. In addition, 20 μm away from the DFB laser cavity, a 50-period second-order grating is defined to couple light out vertically for characterization of the devices on a standard μ-PL setup. Following the epitaxial growth of the GaAs/InGaAs nano-ridges, only a single electron-beam lithography and lift-off step is required to define the grating consisting of a 5 nm/40 nm Ti/Au metal stack on top of the nano-ridges. The Ti layer is added to improve Au adhesion and considered to have negligible impact on the laser performance due to its thin thickness. A positive electron-beam photoresist (AR-P 6200) was used, which results in negative sidewalls, helping with the lift-off of the Au layer even when the very thin electron-beam photoresist ($\sim$ 200 nm) makes the process challenging.

Figure 2(c) shows top-view SEMs of the fabricated devices with the duty cycle Λ_{Au} designed to vary from 0.2 to 0.5 (the sample with duty cycle 0.6 is not shown). The actually measured duty cycles were 0.17, 0.26, 0.37, 0.47 respectively, with the 0.02-0.03 reduction in duty cycle attributed to overexposure.

The fabricated devices are characterized on a μ-PL setup with a Nd:YAG nanosecond pulsed laser pumping the devices from the top. A rectangular aperture is used to limit the pump spot to an area of 3 μm $\times$ 300 μm, covering a single DFB device and maximally excluding adjacent nano-ridges, which have no gratings on top. The pump intensity is controlled by the combination of a polarizer and a rotating half-wave plate (HWP) added in the setup. The measured signal is the diffraction from the second-order-grating coupler, collected by a monochromator with a resolution of 2 nm. A chopper and a lock-in amplifier are used to improve the signal-to-noise ratio.

Figure 4(a) shows the measured spectra of a PLC-DFB device with metallic grating duty cycle of 0.37 pumped at different intensities. When the optical pump power is 9 kW/cm^2 (just below threshold), a broad spectrum centered around 1030 nm with a full width at half maximum (FWHM) of 60 nm is observed. As the pump power increases to 12 kW/cm^2, a peak starts to appear in the spectrum at 1024 nm. Further increase of the pump power to 76 kW/cm^2 ($\sim 6 \times I_{th}$) makes the peak clearer. Finally, at a pump intensity of 417 kW/cm^2 the single peak becomes very distinct reaching around 15 dB above the background. It is believed that the measurement itself suppresses the peak to background ratio of the laser. On the one hand, the peak amplitude is weakened because the second-order grating coupler introduces massive absorption on the lasing wavelength. On the other hand, the background is elevated as the measured signal might also include the PL-signal of two to three as-grown nano-ridges given the fact that they are only $\sim$ 500 nm apart from the DFB device and the pump slit is 3 μm wide at least. Figure 4(b) plots the measured light-in light-out curve (L-L curve) both on a logarithmic and on a linear scale (Fig. 4(b) insert). The output power was integrated over a wavelength range of $\sim$ 5 nm centered at the 1024 nm peak. The distinct single lasing peak and the clear change in the slope of the L-L curve are strong indicators of single-mode laser operation. The threshold is derived to be $\sim$ 10 kW/cm^2 (at an estimated carrier density of 1.69×10^{18}/cm^3), which is even slightly lower than the values obtained for nano-ridge lasers with etched gratings fabricated from the same material [13]. We believe this can be attributed to surface damage introduced by the etching process.

All PLC-DFB devices with duty cycle from 0.2-0.6 showed laser operation. Figure 5(a) displays the lasing spectra of the five devices under a pump intensity of 417 kW/cm^2. Theoretically, the wavelength should remain almost constant for PLC-DFB lasers with the same grating period, regardless of the duty cycle, as the real part of the cavity mode effective refractive index n_{eff} is hardly influenced. Experimentally we find the lasing wavelength varies slightly, we find it to be 1018 nm, 1020 nm, 1024 nm, 1022 nm, 1018 nm for the devices with duty cycle 0.17, 0.26,0.37, 0.46, 0.57 respectively. This discrepancy seems reasonable given the small uncertainty Δn_{eff_b}

Optics EXPRESS

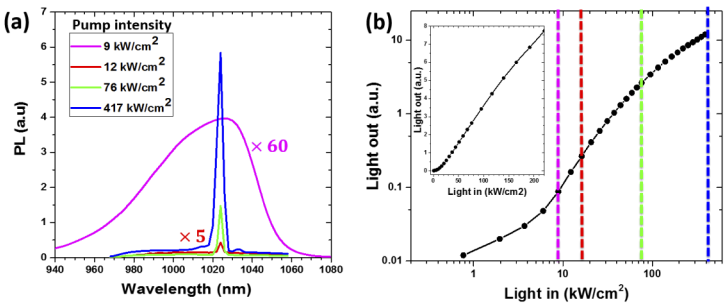

Fig. 4. (a) The spectra of a PLC-DFB laser with grating duty cycle 0.37 under different pump intensities. (b) The Light-in Light-out curve of the same laser at its lasing peak 1024 nm on logarithmic scale. Insert shows the same data plotted in linear scale.

originating from slight variations in the nano-ridge dimensions during the epitaxy process and the limited resolution of the measurement (2 nm).

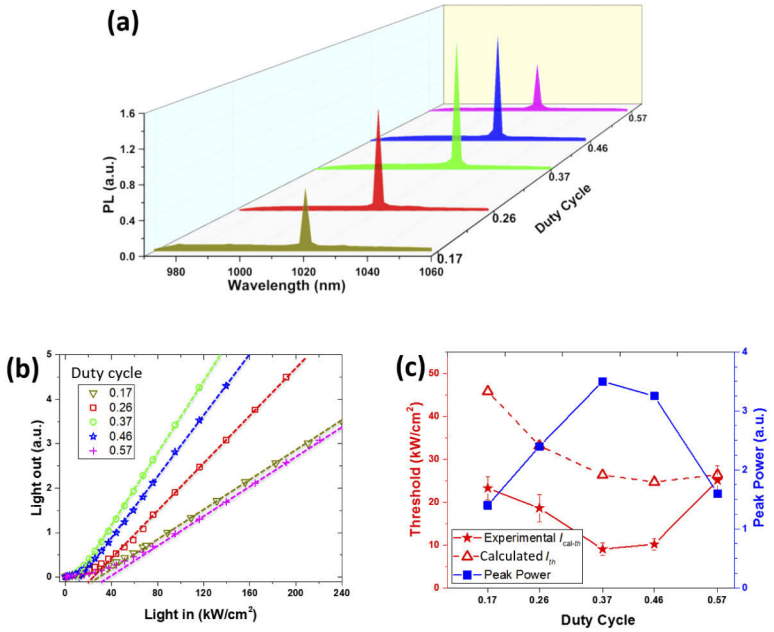

Fig. 5. (a) Spectra of PLC-DFB lasers with grating duty cycle of 0.17, 0.26, 0.37, 0.46, 0.57 respectively, all under 417 kW/cm^2 excitation. (b) The light-in light-out curves for the same devices. The markers indicate the experimental data, the lines are fitted using Eq. (8). (c) Calibrated experimental threshold I_{cal-th}, calculated threshold and peak power of the lasers as a function of grating duty cycle.

The light-in-light-out curves for five devices with different duty cycle are shown in Fig. 5(b) with the dots denoting the experimental data and the dashed lines a fit to the linear part of the curves using:

$$I_{out} = \eta_d \frac{h\nu_{out}}{h\nu_{in}}(I - I_{th}) \tag{8}$$

with η_d the differential quantum efficiency, ν_{in} and ν_{out} the frequency of the pump and lasing light respectively, I_{th} the threshold pump intensity, I the pump intensity and I_{out} the laser output.

Optics EXPRESS

Due to the absorption of the pump in the metal grating, the pump efficiency η_{pump} decreases with duty cycle. It is simulated to be 0.87, 0.84, 0.79, 0.73, 0.67 for duty cycle 0.17, 0.26, 0.37, 0.46, 0.57 respectively. The fitted experimental I_{th} of the lasers is then calibrated (denoted as I_{cal-th} with $I_{cal-th} = I_{th} \times \eta_{pump}$) with the pump efficiency. This calibrated experimental threshold I_{cal-th} is shown in Fig. 5(c) together with the calculated I_{th} and the measured peak power, as function of the duty cycle.

The calibrated experimental I_{cal-th} exhibits a minimal value between duty cycle 0.37 to 0.46, which well matches the calculation of I_{th} with the minimum around duty cycle 0.46. The figure also shows the threshold and peak power exhibit an opposite trend, which means the high-loss and/or low-cavity-coupling-strength devices tend to lose more photons from the cavity and require stronger excitation to lase. However, the value of I_{cal-th} is lower than the calculated I_{th}. The small discrepancy between the experimental and calculated results can be attributed to several reasons. In the calculation of the threshold, the partly loss-coupled cavity was simplified to an index-coupled DFB without facet reflection. Neglecting the loss coupling and the facet reflection simplified the calculation but increases the calculated threshold value. Further, the experimental modal gain is extracted by assuming the pump intensity distribution is uniform. However, the profile of the pump beam is actually Gaussian-like in the VSL measurement, such that the optical gain could be underestimated.

5. Conclusion

In this paper we report the first single-mode, partly loss-coupled DFB InGaAs/GaAs multi-QW nano-ridge lasers monolithically grown on a standard 300-mm Si wafer. Optimising the design of the PLC-DFB cavity allowed to find a favorable trade-off between the cavity loss and the coupling strength introduced by the metallic grating on top of the nano-ridges. Experimentally characterising the optical gain of the as-grown nano-ridges not only demonstrated the high quality of the material but also allowed to develop a model to optimise the devices for lowest threshold. Using a simple processing, we then fabricated PLC-DFB nano-ridge lasers with differing duty cycles. All of them showed single-mode lasing. As expected from the calculations, the device with grating duty cycle 0.4 exhibited the lowest threshold (and the highest output power). These results confirm again the high quality of the III-V nano-ridge grown on Si and provide a first feasibility test for the electrical injection of the nano-ridge lasers through patterned metallic structures on top of the nanoscale waveguide. Facilitating this will require the incorporation of a pin-junction in the nano-ridge however. In addition, the metal contacts might be critical for dissipation of heat generated in the narrow nano-ridge structures during operation.

Finally, although the current emission wavelength around 1020 nm is compatible with coupling to SiN waveguides, a next step is obviously to widen the range of achievable emission wavelengths particularly to the O band (1260 – 1360 nm), e.g. by the growth of InAs quantum dots or by increasing the In content in the QW. The ultimate goal is the demonstration of low-cost, electrically driven lasers monolithically integrated with a standard silicon photonics platform using waferscale processes.

Funding. Fonds Wetenschappelijk Onderzoek (G087317N); Bijzonder Onderzoeksfonds UGent.

Acknowledgements. This work was supported by IMEC's industry-affiliation R&D Program on Optical I/O.

Disclosures. The authors declare no conflicts of interest.

References

1. A. W. Fang, H. Park, O. Cohen, R. Jones, M. J. Paniccia, and J. E. Bowers, "Electrically pumped hybrid algainas-silicon evanescent laser," Opt. Express **14**(20), 9203–9210 (2006).
2. K. Tanabe, K. Watanabe, and Y. Arakawa, "Iii-v/si hybrid photonic devices by direct fusion bonding," Sci. Rep. **2**(1), 349 (2012).
3. G. Roelkens, A. Abassi, P. Cardile, U. Dave, A. de Groote, Y. de Koninck, S. Dhoore, X. Fu, A. Gassenq, N. Hattasan, Q. Huang, S. Kumari, S. Keyvaninia, B. Kuyken, L. Li, P. Mechet, M. Muneeb, D. Sanchez, H. Shao, T. Spuesens, A.

Optics EXPRESS

Subramanian, S. Uvin, M. Tassaert, K. van Gasse, J. Verbist, R. Wang, Z. Wang, J. Zhang, J. van Campenhout, X. Yin, J. Bauwelinck, G. Morthier, R. Baets, and D. van Thourhout, "III-V-on-Silicon Photonic Devices for Optical Communication and Sensing," Photonics **2**(3), 969–1004 (2015).

4. B. B. Bakir, A. Descos, N. Olivier, D. Bordel, P. Grosse, E. Augendre, L. Fulbert, and J. Fedeli, "Electrically driven hybrid si/iii-v fabry-pérot lasers based on adiabatic mode transformers," Opt. Express **19**(11), 10317–10325 (2011).
5. J. Justice, C. Bower, M. Meitl, M. B. Mooney, M. A. Gubbins, and B. Corbett, "Wafer-scale integration of group iii–v lasers on silicon using transfer printing of epitaxial layers," Nat. Photonics **6**(9), 610–614 (2012).
6. A. De Groote, P. Cardile, A. Z. Subramanian, A. M. Fecioru, C. Bower, D. Delbeke, R. Baets, and G. Roelkens, "Transfer-printing-based integration of single-mode waveguide-coupled iii-v-on-silicon broadband light emitters," Opt. Express **24**(13), 13754–13762 (2016).
7. J. Zhang, B. Haq, J. O'Callaghan, A. Gocalinska, E. Pelucchi, A. J. Trindade, B. Corbett, G. Morthier, and G. Roelkens, "Transfer-printing-based integration of a iii-v-on-silicon distributed feedback laser," Opt. Express **26**(7), 8821–8830 (2018).
8. S. Chen, W. Li, J. Wu, Q. Jiang, M. Tang, S. Shutts, S. N. Elliott, A. Sobiesierski, A. J. Seeds, I. Ross, P. Smowton, and H. Liu, "Electrically pumped continuous-wave iii–v quantum dot lasers on silicon," Nat. Photonics **10**(5), 307–311 (2016).
9. D. Jung, Z. Zhang, J. Norman, R. Herrick, M. Kennedy, P. Patel, K. Turnlund, C. Jan, Y. Wan, A. C. Gossard, and J. Bowers, "Highly reliable low-threshold inas quantum dot lasers on on-axis (001) si with 87% injection efficiency," ACS Photonics **5**(3), 1094–1100 (2018).
10. M. E. Groenert, C. W. Leitz, A. J. Pitera, V. Yang, H. Lee, R. J. Ram, and E. A. Fitzgerald, "Monolithic integration of room-temperature cw gaas/algaas lasers on si substrates via relaxed graded gesi buffer layers," J. Appl. Phys. **93**(1), 362–367 (2003).
11. T. Mårtensson, C. P. T. Svensson, B. A. Wacaser, M. W. Larsson, W. Seifert, K. Deppert, A. Gustafsson, L. R. Wallenberg, and L. Samuelson, "Epitaxial iii- v nanowires on silicon," Nano Lett. **4**(10), 1987–1990 (2004).
12. Y. Han, W. K. Ng, Y. Xue, Q. Li, K. S. Wong, and K. M. Lau, "Telecom inp/ingaas nanolaser array directly grown on (001) silicon-on-insulator," Opt. Lett. **44**(4), 767–770 (2019).
13. Y. Shi, W. Guo, J. Van Campenhout, Z. Wang, M. Pantouvaki, D. Van Thourhout, and B. Kunert, "Optical pumped InGaAs/GaAs nano-ridge laser epitaxially grown on a standard 300-mm Si wafer," Optica **4**(12), 1468–1473 (2017).
14. D. Van Thourhout, Y. Shi, M. Baryshnikova, Y. Mols, N. Kuznetsova, Y. De Koninck, M. Pantouvaki, J. Van Campenhout, R. Langer, and B. Kunert, "Chapter eight - nano-ridge laser monolithically grown on (001) si," in *Future Directions in Silicon Photonics*, vol. 101 of *Semiconductors and Semimetals* S. Lourdudoss, J. E. Bowers, and C. Jagadish, eds. (Elsevier, 2019), pp. 283–304.
15. B. Kunert, W. Guo, Y. Mols, B. Tian, Z. Wang, Y. Shi, D. V. Thourhout, M. Pantouvaki, J. V. Campenhout, R. Langer, and K. Barla, "Iii/v nano ridge structures for optical applications on patterned 300 mm silicon substrate," Appl. Phys. Lett. **109**(9), 091101 (2016).
16. B. Kunert, W. Guo, Y. Mols, R. Langer, and K. Barla, "Integration of iii/v hetero-structures by selective area growth on si for nano-and optoelectronics," ECS Trans. **75**(8), 409–419 (2016).
17. Y. Shi, B. Kunert, Y. De Koninck, M. Pantouvaki, J. Van Campenhout, and D. Van Thourhout, "Novel adiabatic coupler for iii-v nano-ridge laser grown on a si photonics platform," Opt. Express **27**(26), 37781–37794 (2019).
18. K. David, J. Buus, and R. G. Baets, "Basic analysis of ar-coated, partly gain-coupled dfb lasers: The standing wave effect," IEEE J. Quantum Electron. **28**(2), 427–434 (1992).
19. K. David, J. Buus, G. Morthier, and R. Baets, "Coupling coefficients in gain-coupled dfb lasers: Inherent compromise between coupling strength and loss," IEEE Photonics Technol. Lett. **3**(5), 439–441 (1991).
20. "Bragg grating initial design with fdtd," https://apps.lumerical.com/pic_passive_bragg_initial_design_with_fdtd.html. Accessed: 2010-09-30.
21. G. Morthier and P. Vankwikelberge, *Handbook of distributed feedback laser diodes* (Artech House, 2013).
22. S. L. Chuang, *Physics of photonic devices*, vol. 80 (John Wiley & Sons, 2012).
23. K. L. Shaklee and R. F. Leheny, "Direct determination of optical gain in semiconductor crystals," Appl. Phys. Lett. **18**(11), 475–477 (1971).
24. K. L. Shaklee, R. E. Nahory, and R. F. Leheny, "Optical gain in semiconductors," J. Lumin. **7**, 284–309 (1973).
25. T. C. Chong and C. G. Fonstad, "Theoretical gain of strained-layer semiconductor lasers in the large strain regime," IEEE J. Quantum Electron. **25**(2), 171–178 (1989).
26. S. R. Chinn, P. S. Zory, and A. R. Reisinger, "A model for grin-sch-sqw diode lasers," IEEE J. Quantum Electron. **24**(11), 2191–2214 (1988).